The effect of Nb/Ti ratio on hardness in high-strength Ni-based superalloys

Hisazawa, Hiromu; Terada, Yoshihiro; Adziman, Fauzan; Crudden, David J.; Collins, David M.; Armstrong, David E J; Reed, Roger C.

DOI:
10.3390/met7030071

Document Version
Publisher's PDF, also known as Version of record

Citation for published version (Harvard):
Hisazawa, H, Terada, Y, Adziman, F, Crudden, DJ, Collins, DM, Armstrong, DEJ & Reed, RC 2017, 'The effect of Nb/Ti ratio on hardness in high-strength Ni-based superalloys', *Metals*, vol. 7, no. 3, 71. https://doi.org/10.3390/met7030071

metals

MDPI

Article

The Effect of Nb/Ti Ratio on Hardness in High-Strength Ni-Based Superalloys

Hiromu Hisazawa [1,*], Yoshihiro Terada [2], Fauzan Adziman [3], David J. Crudden [3], David M. Collins [3], David E. J. Armstrong [4] and Roger C. Reed [4]

1 Department of Materials Science and Engineering, Interdisciplinary Graduate School of Science and Engineering, Tokyo Institute of Technology, Yokohama 226-8502, Japan
2 Department of Materials Science and Engineering, School of Materials and Chemical Technology, Tokyo Institute of Technology, Yokohama 226-8502, Japan; terada.y.ab@m.titech.ac.jp
3 Department of Engineering Science, University of Oxford, Parks Road, Oxford OX5 1PF, UK; fauzan.adziman@eng.ox.ac.uk (F.A.); david.crudden@materials.ox.ac.uk (D.J.C.); david.collins@materials.ox.ac.uk (D.M.C.)
4 Department of Materials, University of Oxford, Parks Road, Oxford OX5 1PF, UK; david.armstrong@materials.ox.ac.uk (D.E.J.A.); roger.reed@eng.ox.ac.uk (R.C.R.)
* Correspondence: hisazawa.h.aa@m.titech.ac.jp; Tel.: +81-45-924-5617

Academic Editor: Jonathan Cormier
Received: 12 January 2017; Accepted: 20 February 2017; Published: 23 February 2017

Abstract: The age-hardening behaviour and microstructure development of high strength Ni-based superalloys ABD-D2, D4, and D6 with varying Nb/Ti ratios have been studied. The studied alloys have large volume fractions and multimodal size distributions of the γ' precipitates, making them sensitive to cooling conditions following solution heat treatment. Differential scanning calorimetry was conducted with a thermal cycle that replicated a processing heat treatment. The hardness of these alloys was subsequently evaluated by nanoindentation. The Nb/Ti ratio was not observed to influence the size and distribution of primary and secondary γ' precipitates; however, the difference in those of tertiary γ' and precipitate morphology were observed. The nanoindentation hardness for all alloys reduces once they have been solution-heat-treated. The alloys exhibited specific peak hardness. The alloy with the greatest Nb content was found to have the best increase in hardness among the alloys studied due to its large tertiary γ' precipitate.

Keywords: superalloy; nanoindentation; age-hardening; Nb/Ti ratio

1. Introduction

To satisfy increasing aerospace emissions targets [1], gas turbine engine efficiency needs to be improved. The high temperature mechanical properties and oxidation resistance of the materials selected for use in such application largely limit performance. Currently, nickel-based superalloys are used in the sections of the engine that experience high static stress at elevated temperatures—in particular, turbine discs that rotate at 10,000 rpm or greater; these alloys work very closely to their limit of tolerance of temperature or stress [2]. One of the ways in which the performance of gas turbine engines could be improved is by developing new nickel-based superalloys that could operate under more demanding conditions.

Nickel-based superalloys typically comprise a face-centered-cubic (A1) matrix (γ) solid solution that is strengthened with a dispersion of coherent intermetallic precipitates (γ') with an $L1_2$ crystal structure. During alloy development, the compositions selected are critical, as this will ultimately determine the performance of the material, irrespective of process optimization and its relationship. The effect of different γ' precipitate formers, Al, Ti, Ta, and Nb on the microstructure and mechanical

properties in nickel-base superalloys, has been a subject of considerable research [3–6]. For example, the Ti/Al ratio is known to raise the anti-phase boundary (APB) energy of γ' [3] and increase the lattice misfit between the γ and γ' phases [4,5]. Whilst Al has predominantly been used as the γ' former in nickel-based superalloys, Nb has also been used; however, it has been reported to have a limited effect on the γ–γ' lattice misfit [6]. Nb additions will increase the γ' volume fraction and will act as a potent solid solution strengthening element in γ [7]. The effect of combining Ti and Nb is less well known.

Recently, Reed et al. [8] and subsequently Zhu et al. [9] have suggested and employed a systematic alloy composition design procedure. As a part of this design process, they developed several indices for important characteristics, such as creep resistance, density, and cost with a physical understanding between each characteristic and the composition, and new alloys could be selected. However, in terms of this design, Ti and Nb have some similar characteristics to predict the performance of the alloys. Table 1 summarizes a comparison between Ti and Nb in terms of alloy design. Although Ti is a third-row element and Nb is the fourth-row element, they both have the same order of diffusion coefficients in A1–Ni, Vegard coefficients, and metal-d levels. The diffusion coefficient is an important parameter for predicting precipitate coarsening rates and creep resistance. The Vegard coefficient is often used for predicting lattice parameter and lattice misfits; an important parameter that influences coarsening behaviour of γ' precipitates. Metal-d levels are also an important parameter because they are used in simplified estimates of the topologically close-packed (TCP) phase probability, which is developed by elementary band theory [10]. The TCP phase is well associated with the formation of voids, which may potentially act as initiation sites for fractures [11,12].

Table 1. Comparison between the design parameters for alloys containing Ti and Nb.

Parameters	Titanium	Niobium
Atomic number	22	41
Period	4	5
Melting point of pure metal	1941 K	2750 K
Atomic radius	0.160 nm	0.146 nm
Diffusion coefficient in A1–Ni at 1173 K [2]	5×10^{-16} $m^2 \cdot s^{-1}$	3×10^{-16} $m^2 \cdot s^{-1}$
Vegard coefficient for $L1_2$–Ni_3Al [2]	2.5×10^{-4} nm/atom %	4.5×10^{-4} nm/atom %
Metal-d levels [10]	2.271 eV	2.117 eV

Microstructures of the alloys for the turbine discs are relatively complex. They can show up to three distinct or more generations of γ' precipitates, with different size ranges, compositions, and precipitation processes each with a different effect on the mechanical properties [13]. Precipitates mostly found at grain boundaries are termed primary γ' and have a diameter of approximately 1 μm. Finer secondary and tertiary γ' precipitates are approximately ~100 nm and ~50 nm in diameter, respectively. Primary γ' precipitates form during alloy manufacturing and processing procedures such as castings and forgings. Secondary and tertiary γ' precipitates form during the cooling from temperatures of solution treatment and through subsequent ageing heat treatments; they form as a result of the competition between the nucleation and growth of the γ' precipitates [13–15]. The cooling conditions from a solution temperature has a great influence on the initial γ' distributions, the subsequent ageing response, and the resulting mechanical properties; careful attention therefore needs to be paid to them in order to understand them.

The plastic deformation of coherent superlattice γ' precipitates require either the shearing of paired dislocations (i.e., leading and trailing dislocations) or the bypassing of a dislocation. It is well established that the shearing of the γ' precipitates is the main contributor to the strength of polycrystalline superalloys, as replicated by a dislocation pair model [16,17]. The models describe that interfacial energy associated with an APB is created by a leading dislocation minimised by the passage of the trailing dislocation. This model considers interactions between dislocation pairs with small (weak pair coupling) and large (strong pair coupling) precipitates with a unimodal size distribution and a low volume fractions of γ' precipitates. Jackson and Reed [18] and subsequently Collins and Stone [19]

have employed the weak and strong pair models in the optimization of the microstructures in Udimet 720Li and RR1000, respectively. Their analyses were based on the optimal γ' size where transitions between the weak and strong pair couplings occurred. The maximised critical resolved shear stress (CRSS) is achieved at the optimal size, and it is strengthened by the larger APB energy and volume fractions of the γ' precipitates. The dislocation pair model was extended by Galindo-Nava et al. [20] so as to apply to a multimodal particle distribution; they succeeded in predicting the effect of tertiary γ' precipitates on CRSS, which demonstrates a possibility of improve the mechanical properties of a superalloy. Consequently, the yield behaviour of nickel-based superalloys is strongly influenced by the size distributions and volume fractions of the secondary and tertiary γ' precipitates, whilst the role of the primary γ' is limited to grain boundary pinning, which minimises the growth of γ grains during solution heat treatment. Understanding how to control the secondary and tertiary γ' phases are crucial to maximising the mechanical properties of Ni-based superalloys.

In this study, a range of model alloys are investigated in order to systematically study the effect of Ti and Nb on γ' precipitation and its effect on a simple mechanical property: hardness. In particular, the comparative effects of Ti and Nb on multimodal γ' precipitates size distributions are characterised and compared in this study.

2. Materials and Methods

2.1. Materials

ABD series alloys were used in this study. They are polycrystalline nickel-based superalloys and were manufactured by ATI Powder Metals using a lab-scaled version of a commercial powder metallurgy process. Three different alloys containing varying concentrations of Ti (2.8–4.1 atom %) and Nb (0–1.2 atom %) with these elements are substituted on a 1:1 basis. The nominal composition of each alloy (atom %) is listed in Table 2. A high-temperature synchrotron X-ray diffraction study has been reported in a previous study [21]. The lattice misfits of D2, D4, and D6 are positive at temperatures below 1273 K, i.e., the lattice parameter of the γ' precipitate is larger than that of the γ matrix, whose values for D2, D4, and D6 are approximately 0.07%, 0.09%, and 0.10% at 1123 K, respectively. These alloys have a 40%–45% volume fraction of γ' precipitates at 1123 K. The specimens were received after forging and cut into 1-mm-thick square plates that have dimensions of $2.5 \times 2.5\ mm^2$ using electro-discharge machining (Brother industries, Ltd., Nagoya, Japan) and a high-speed precision cutting machine (Heiwa Technica, Zama, Japan, and Struers Ltd., Rotherham, UK). The weight was approximately 0.2 g.

Table 2. The nominal alloy compositions in this study (atom %).

Alloy	Ni	Cr	Co	Mo	W	Al	Ti	Ta	Nb	C	B	Zr
D2	Bal.	18.7	18.2	0	0.9	8	4.1	0.6	0	0.127	0.078	0.037
D4	Bal.	18.7	18.2	0	0.9	8	3.6	0.6	0.4	0.127	0.078	0.037
D6	Bal.	18.7	18.2	0	0.9	8	2.8	0.6	1.2	0.127	0.078	0.037

2.2. Heat Treatment

Ni-based superalloys with large volume fractions of γ' precipitates have a strong driving force for precipitation and quite fast precipitation kinetics. The microstructural and mechanical properties of the alloys are very sensitive to solvus temperature and cooling rates following heat treatment [20,22]. Accurate control and homogeneity of the specimen temperature were achieved through the use of a differential scanning calorimeter (DSC) NETSZCH DSC404F1 (NETZSCH Analyzing & Testing, Wolverhampton, UK) for a small specimen in an argon flow. A thermal process typical of a 1 step super-solvus treatment, which is used for current generation turbine disc alloys, and isothermal ageing at 1123 K were conducted on each alloy studied. The rate of heating from room temperature to approximately 30 K above the γ' solvus temperature was controlled to be $10\ K{\cdot}min^{-1}$. The subsequent

cooling rate was controlled so as to fall to 673 K at a rate of 1 K·min^{-1}. The solution temperatures of the alloys were studied by DSC and approximately confirmed by synchrotron X-ray diffraction [21]. Figure 1 shows the set and measured temperatures together with a typical DSC trace for alloy D2. The other alloys had similar results. The temperature was precisely controlled during cooling to 973 K, at which point significant microstructure change was deemed to be negligible. We also confirmed precipitation of the γ' phase corresponding to two exothermal peaks, one at 1230 K for the formation of secondary γ' and the other at 1060 K for the formation of tertiary γ'.

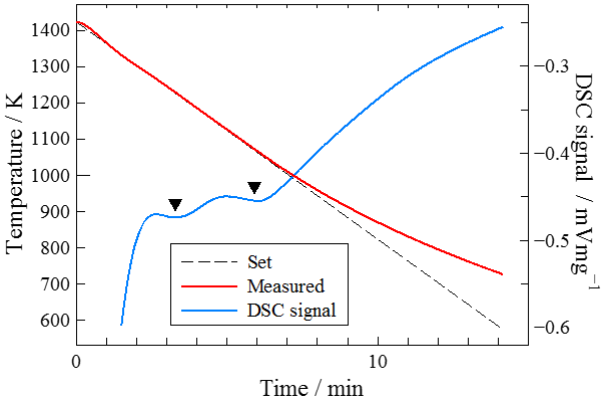

Figure 1. Set and measured temperatures of the D2 alloy together with a typical DSC spectrum; the black downward-pointing triangles indicate exothermal peaks consistent with γ' precipitation. The other alloys used in this study exhibited similar results.

2.3. Microstructure Observation

To prepare the specimens for microstructure observations, any surface oxide produced by the heat treatment was removed using abrasive media. Microstructure observations were conducted by using a field-emission scanning electron microscope (FE-SEM) (JEOL Ltd., Akishima, Japan) with an accelerating voltage of 15 kV. The specimens analysed by the FE-SEM were prepared using both a traditional metallographic technique and chemical–mechanical polishing by a diluted colloidal silica. Electrolytic etching was performed with phosphoric acid saturated with chromium oxide (VI). The particle size of the γ' precipitate was also measured using an SEM secondary electron image (SEM-SEI). It is noted that the electrolytic etching dissolves the γ matrix, leaving γ' precipitates in relief; this results in the γ' volume fraction being over-estimated and the particle size being underestimated due to overlapping particles. Nevertheless, it is reasonable for us to evaluate the shape of the projected γ' particles stereologically.

2.4. Nanoindentation

The samples in this study were prepared using DSC; thus, the size of the specimens was limited. It is therefore difficult to reveal the mechanical properties of the samples using conventional testing methods such as a tensile test or even Vickers hardness test. As such, nanoindentation experiments were performed in this study at room temperature. The samples that studied with nanoindentation were also prepared using both a conventional metallographic technique and polishing with diluted colloidal silica. In all of the indentation experiments, a Berkovich tip with a tip angle of 65.3° was used. The load and corresponding displacement were recorded continuously during the indentation. The indentation hardness H_{IN} was derived from the nanoindentation experiments using the following equation:

$$H_{IN} = \frac{F}{A(h)} \approx \frac{F}{26.43h^2} \quad (1)$$

where F is the applied load, $A(h)$ is the projected contact area at that load, and h is the penetration depth. An empirical constant of 26.43 used in Equation (1) is a constant dependent on the indenter shape. The indentation hardness at the maximum depth was selected as being the representative hardness, because at a small depth it might be hardened by either the scale effect or the surface roughness. The maximum h was kept at a constant 2000 nm and the strain rate was kept at 0.1 s^{-1}. The depth of 2000 nm corresponds to an indent width of 15 μm, which is sufficiently smaller than the specimen used but larger than the γ′ precipitates. We therefore expect that the hardness measurements are from a volume that is representative of the material, containing the full tri-modal γ′ precipitate distribution.

3. Results

3.1. Initial Microstructure

In this study, all of the specimens have a typical multimodal distribution of γ′ precipitates. Figure 2 shows micrographs of the as-received (as-forged), and solution-heat-treated specimens. The as-solution-treated D2, D4, and D6 alloys show similar microstructures. The as-received specimens were found to have a heterogeneous grain size, which could be attributed to the heterogeneity of the manufacturing process. The alloys also have large area fractions and densities of primary precipitates at both the grain boundary and the grain interior (Figure 2a). The primary γ′ precipitates almost dissolves into the matrix during the solution heat treatment. As there is almost no primary γ′ precipitates, the γ grain grew dramatically; uniform grain sizes could be obtained. The solution treatment enabled us to obtain a homogeneous microstructure (Figure 2b). After the solution treatment and cooling, we can observe that the residual primary γ′ particles have a diameter of ~1 μm, the secondary γ′ particles have a diameter of ~200 nm, and very fine tertiary γ′ particles have a diameter of less than 50 nm. (Figure 2c). The primary γ′ particles show a lenticular shape and are dispersed along the grain boundaries. The solution heat treatment temperatures were selected to be supersolvus in order to dissolve the primary γ′ completely; in fact, the temperature of the real solvus is slightly above the solution heat treatment temperatures. The volume fraction of the primary γ′ observed from the FE-SEM is less than 1%. There are two types of secondary γ′ particles are observed. Some of the secondary particles are granular, but the others are flower-like or irregular morphologies. The tertiary γ′ particles are dispersed around both the γ grain boundary and the primary γ′ particles, and they form "pools of tertiary γ". Very few tertiary γ′ are observed in the vicinity of the secondary precipitates. The area fraction of the pool or intragranular tertiary γ′ is also less than 3% of the total observed area. No distinct differences were found between the alloys in terms of their microstructures.

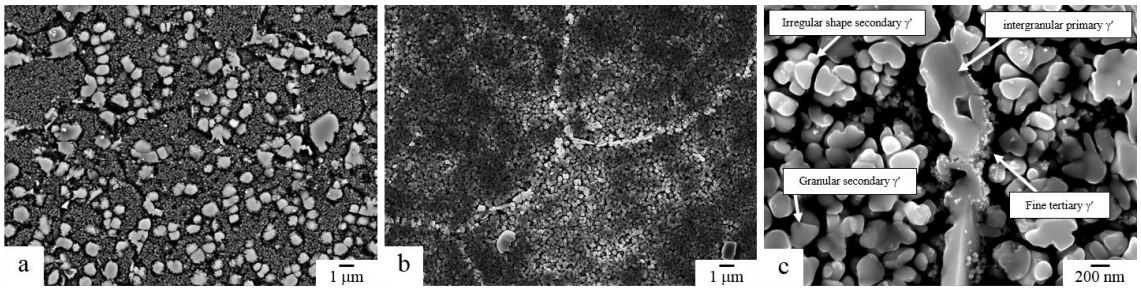

Figure 2. Microstructures of the D2 alloy as-received (**a**), as-solution-heat-treated (**b**), and as-solution-treated viewed at high magnification (**c**).

3.2. Microstructure Evolution with Aging

Figure 3 shows the microstructures of each alloy aged at 1123 K for 8 h. Despite a sufficiently long aging heat treatment, there is no distinct difference between the microstructures with varying Nb/Ti ratios or aging at 1123 K. No coarsening is observed for the primary or secondary γ′ precipitates. The shape of the secondary γ′ precipitates, however, seems to change slightly; this is discussed in

greater detail in Section 4.1. Figure 4 shows the secondary γ′ particles in the D4 alloy aged at 1–8 h at 1123 K. After 1 h aging, γ′ particles tend to form granular shapes, but by 8 h some of the precipitates form an irregular shape. Irregularly shaped precipitates form "dents" as a result of morphological change (see arrows in Figure 4c). Secondary γ′ precipitates slightly coarsen with aging heat treatment, but without significant change. Differences in the microstructures of the samples with Nb/Ti ratio are not observed for the secondary γ′ particles.

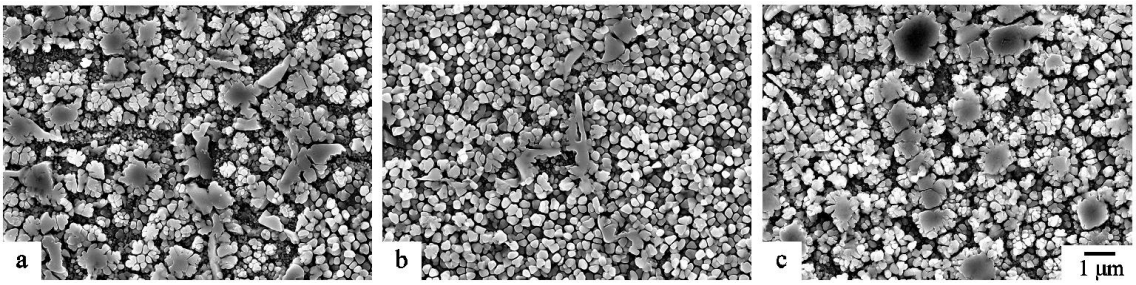

Figure 3. Microstructures of the D2 (**a**), D4 (**b**), and D6 (**c**) alloys after aging at 1123 K for 8 h.

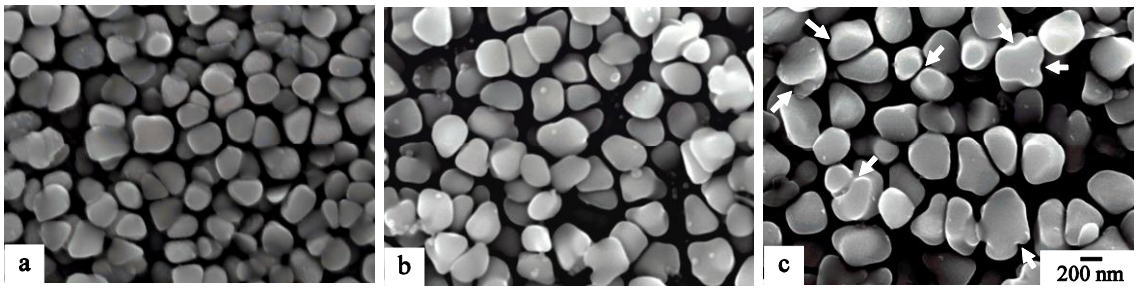

Figure 4. Morphological evolution of the secondary γ′ precipitates after aging at 1123 K for 1 h (**a**), 4 h (**b**), and 8 h (**c**) in the D4 alloys. The precipitates tend towards irregular-shape morphology rather than a granular shape as the aging increased. The arrows in (**c**) indicates "dents" of the γ′ particles.

In contrast, the tertiary γ′ precipitates show a clear difference in their distribution. Figure 5 shows pools of the tertiary γ′ particles in specimens aged for 1 h and 8 h. For the 1 h aged specimens, tertiary γ′ particles have a diameter of approximately 30 nm, and there are no significant differences observed between the three alloys. The volume fractions of the tertiary γ′ precipitates cannot be measured using a microscope, but they are roughly the same for all alloys. However, the size of those precipitates rapidly coarsens with aging. The average diameter of the tertiary γ′ particles reach around 80 nm for D2 (Nb/Ti = 0) and 150 nm for D6 (Nb/Ti = 2); these results suggest that Nb might accelerate the growth rate of the tertiary γ′ particles, despite having a negligible effect on the initial particle size.

Figure 6 shows a change in the particle size of the primary (a), secondary (b), and tertiary γ′ (c) precipitate following heat treatment. The precipitate sizes were evaluated with a radius of an area-equivalent circle; the primary γ′ precipitates are >400 nm; the secondary γ′ precipitates are 100–400 nm; the tertiary γ′ precipitates are <100 nm. As mentioned above, the size of the primary and secondary γ′ precipitates are always 800 and 200 nm, respectively, and they grow slightly after 8 h aging. They clearly do not raise to the power 1/3 with respect to time, which is often observed in superalloys [23]. The tertiary γ′ precipitates show more rapid growth rates, which are faster in the alloys that have greater Nb/Ti ratios.

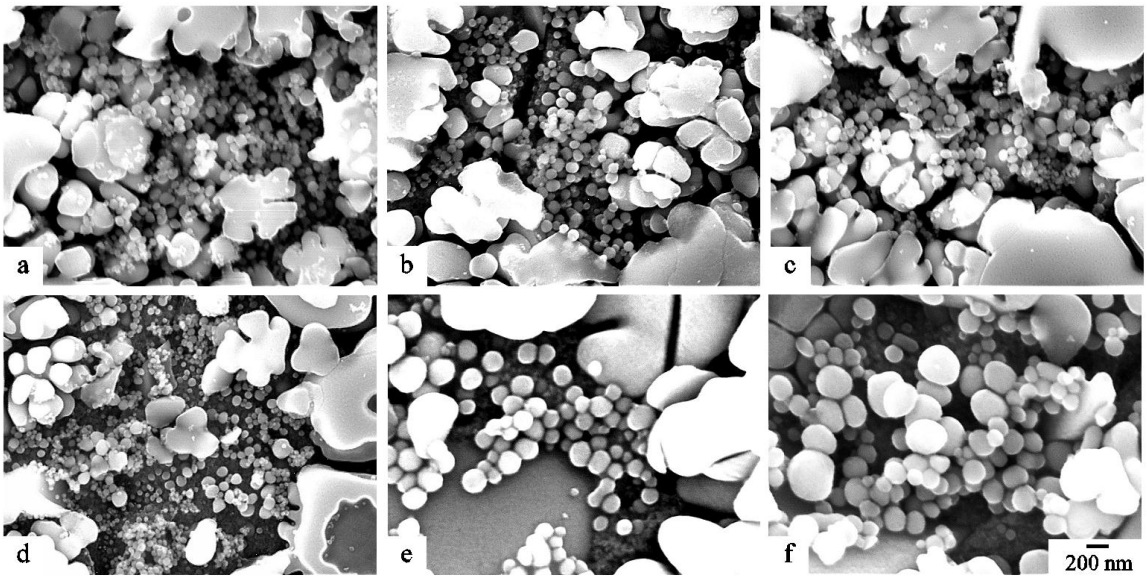

Figure 5. The pool of tertiary γ′ precipitates observed in the D2 (**a**,**d**), D4 (**b**,**e**), and D6 (**c**,**f**) alloys aged at 1123 K for 1 h (**a**–**c**) and 8 h (**d**–**f**).

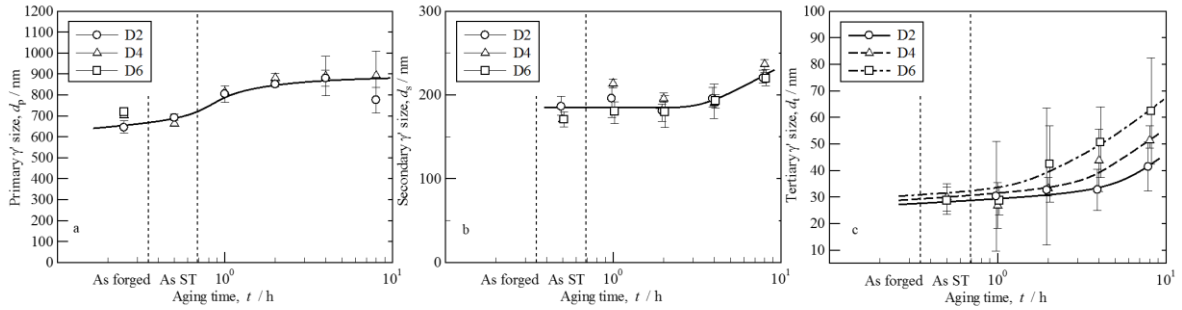

Figure 6. Changes in the particle size of the primary (**a**), secondary (**b**), and tertiary (**c**) γ′ particles of ABD alloys following forging, solution treatment, and isothermal aging at 1123 K.

3.3. Nanoindentation Hardness

To evaluate what effects of the microstructures on the mechanical properties of the alloys, nanoindentation hardness measurement was performed. Figure 7 shows the changes in nanoindentation hardness of the D2, D4, and D6 alloys following heat treatment. The as-received specimens with varying Nb/Ti ratios show different hardnesses due to the grain size heterogeneity and coarse primary γ′ precipitates described in Figure 2. The difference in hardness is eliminated by solution heat treatment resulting in the same hardness of 3.9 GPa for each alloy. Following the aging treatment, the alloys show typical age-hardening curves, i.e., the hardness increases during precipitation and growth and decreases when the coarsening of the γ′ precipitate process dominates. The peak aging time is approximately 4 h for all of the alloys, but the peak hardness increases as the Nb/Ti ratio increases. The D6 alloy, which has an Nb/Ti ratio of 2, exhibits the highest hardness (4.2 GPa). The behaviour of the age-hardening process will be discussed in a Section 4.2.

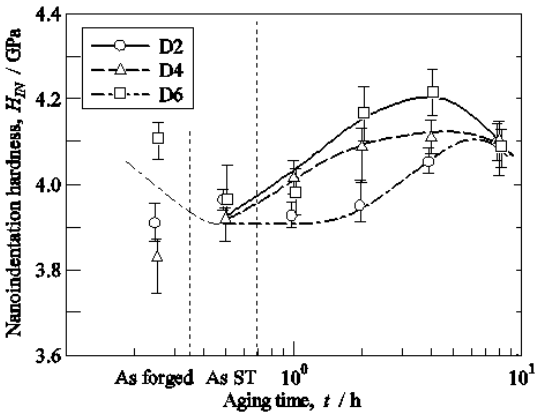

Figure 7. Measured nanoindentation hardness of the ABD alloys following heat treatment: forging, solution treatment, and isothermal aging at 1123 K.

4. Discussion

4.1. The Effect of the Nb/Ti Ratio on the Multimodal Distribution of the γ′ Precipitates

Nb and Ti were substituted for the ABD series alloy, and the effect of this on a microstructure of the alloys has been examined. The D2 alloy has the lowest Nb/Ti ratio, the D6 alloy has the highest, and D4 has a ratio that is in the middle of the two. All of the alloys have almost the same mean precipitate sizes and densities of relatively coarse primary and secondary γ′ precipitates. A previous study [19] revealed that the volume fractions of γ′ precipitate do not differ significantly between these alloys. They also have similar size of tertiary γ′ precipitate just after the solution heat treatment and cooling as described in Figure 6. Sarosi et al. [14] have suggested that the multimodal distributions of γ′ precipitates form due to competition between the nucleation and growth of γ′ precipitates; they predict that a monomodal distribution would be obtained when the growth rate is much faster than the nucleation, and the precipitation would have a wider size distribution when the nucleation is faster. A multimodal distribution can be obtained only when the kinetics of both processes are equivalently fast. There is no significant difference in size distributions of γ′ precipitates regardless of Nb/Ti ratio, which suggests that the Nb/Ti ratio does not have a significant influence on the nucleation and growth kinetics during cooling from solution temperature. This is not surprising because the Nb–Ti diffusion rate in the matrix and the thermodynamic stability of the γ′ phase are similar.

During aging at 1123 K, the mean size of primary and secondary γ′ precipitates do not change. The primary γ′ precipitates remained quite large, with little coarsening observed. However, Figure 5 shows the morphological change of the secondary γ′ precipitates, which may have occurred due to directional coarsening, which has been reported by Ricks [24] and Qiu et al. [25]. This may also have been due to cyclic and reversal coarsening reported by Chen et al. [26]. It is more likely that the morphological change is due to cyclic coarsening, because the coarsening direction of the precipitates appears to be related to the orientation of the grain where they are situated. The unchanged size of the secondary γ′ particles can also be explained by cyclic coarsening. Figure 8 shows additional evidence of the cyclic coarsening phenomenon. During the microstructure observation, granular-shape precipitates (Figure 8a) were observed over almost the entire area of the specimen, but irregular-shape precipitates (Figure 8b) were observed in some locations within the γ grain. A few residual intragranular γ′ particles show an irregular shape (Figure 8c), which may have been a result of the growth and splitting of the γ′ precipitates. The "humps" of the intragranular primary γ′ particles are similar in size to that of the secondary γ′ precipitates, and we estimated the maximum precipitate size under the constraint of a lattice misfit. The coarsening direction depends on the elastic interaction between particles. In other words, the morphological change is a result of the directional coarsening in conjunction with the bypassing of the elastic field generated by neighboring particles and of their own splitting [27].

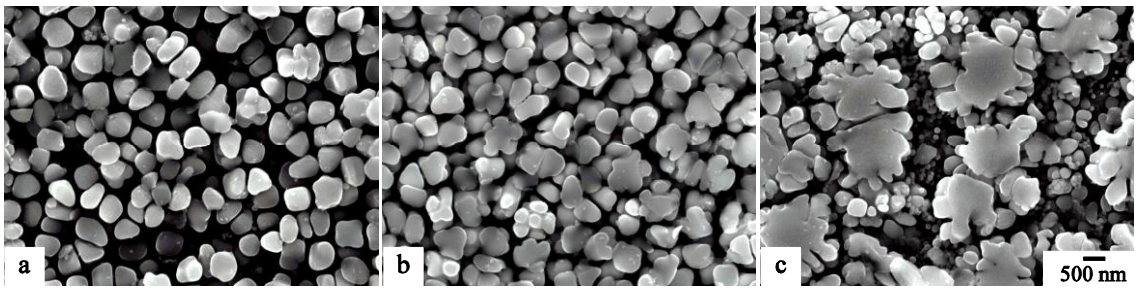

Figure 8. Microstructures of the D4 alloy aged at 1123 K for 1 h showing microstructure heterogeneity: Granular-shaped precipitates (**a**), irregular-shape precipitates (**b**), and residual intragranular precipitates (**c**).

Only the tertiary γ' precipitates are influenced by the Nb/Ti ratio, and the alloys with higher Nb/Ti ratios show faster growth rates of the tertiary γ' precipitates. The differences between the growth rates are not simply attributed to the diffusion rate; Nb has a similar or slightly smaller diffusion coefficient than that of Ti. The other potential reason for the difference is related to the partitioning of the Nb and Ti between the matrix and the precipitate. For instance, the Nb would be enriched near the pools of tertiary γ' particles and would enhance the growth of the tertiary γ' if the Nb is in the partitioned matrix around the solution temperature. A compositional study is therefore needed in order to reveal the reason why the tertiary precipitates grow faster in the D6 alloy. However, it is very difficult to analyse the composition around the tertiary γ' particles because of a requirement of high spatial resolution and accuracy.

4.2. Age Hardening Behaviour of the ABD Alloys

The Nb/Ti ratio does not influence the nanoindentation hardness of the solution-treated alloys; however, it impacts the subsequent age hardening behaviour. The alloys with higher Nb/Ti ratios show higher peak aging hardness. It is known that precipitate shearing is the main deformation mechanism in alloys for turbine discs [17], and it is expected that Nb would have a significant effect on the APB energy, lattice misfit, microstructure, volume fraction of the γ' precipitates, and several other factors influencing strength. However, a previous study of X-ray synchrotron diffraction [21] shows that the lattice misfit almost never changes and that the volume fraction slightly increases as the Nb/Ti ratio increases. Because the hardness increased with volume fraction, this reported tendency contrasts with our experimental result. It is likely that the solid solution strengthening of the matrix and the increase in APB energy by Nb in the γ' precipitate is negligible because the hardness of the solution-treated alloys are similar. The alloys that have different Nb/Ti ratios show similar microstructures, except for the size of tertiary γ' precipitate, as mentioned in Section 4.1.

We can therefore see that the growth of tertiary γ' precipitate is the most potent factor for improving age-hardening ability. Jackson and Reed [18] have shown that the tertiary γ' precipitates play an important role in the mechanical property of Udimet 720Li, and Galindo-Nava et al. [20] demonstrated that small amounts of fine tertiary γ' precipitates are able to significantly strengthen the CRSS in Udimet 720Li. The area fraction of the pool of tertiary γ' precipitates is less than 3%; however, intragranular tertiary γ' is not observed; it is possible that they were washed out by the electrolytic etching. The fact that only a small amount of tertiary γ' is required to improve the hardness of the alloys encourages us to investigate the process of a multimodal distribution of γ' precipitates and its dependence on the composition, such as the Nb/Ti ratio.

5. Conclusions

In this study, the effect of Nb/Ti ratio on the microstructure formation and hardness during a typical solution treatment and aging is investigated in high strength superalloys. We were able to

precisely control the cooling rates from the solution heat treatment, which enabled us to evaluate the role of Nb and Ti in the formation of multimodal distributions of γ' precipitates. Our conclusions are summarised as follows:

- Near-supersolvus solution-treated and cooled alloys show multimodal distributions of γ' precipitates containing relatively coarse primary and secondary γ' precipitates at the grain boundary and interior, respectively, and fine tertiary γ' precipitates form a pool of them around the grain boundary or primary γ' precipitates.
- All of the alloys studied show typical age-hardening behaviour at 1123 K, but higher peak hardness is obtained in the alloys that have higher Nb/Ti ratios.
- The microstructures of solution-treated alloys are similar and imply that they are independent of the Nb/Ti ratio; however, faster growth rates are observed for the tertiary γ' precipitate in the alloy with higher Nb/Ti ratios. Larger tertiary γ' precipitate are believed to be the reason why the higher hardness of the alloys studied.
- The Nb/Ti ratio does not influence the morphologies of primary and secondary precipitates, but it does influence tertiary γ' precipitates; this might be due to Nb and Ti partitioning at high temperatures.
- Several pieces of the evidences are observed for cyclic coarsening or splitting in all of the alloys. The size of the secondary γ' precipitates remained constant, which might be due to cyclic coarsening of the precipitates.

Acknowledgments: The authors wish to thank Paraskevas Kontisa, Enrique Alabort, and André Németh for experimental support and good discussion. This work was supported by a Grant-in-Aid for JSPS Research Fellow Number JP2611840, Japan and in part by Program for Leading Graduate Schools "Academy for Co-creative Education of Environment and Energy Science", MEXT, Japan.

Author Contributions: D.J. Crudden, D.M. Collins, and R.C. Reed designed the experiments and supplied the materials; H. Hisazawa performed the experiments, analysed the data, and wrote the paper; D.E.J. Armstrong contributed nanoindentation experiments; F. Adziman and Y. Terada support to writing this paper.

Conflicts of Interest: The authors declare no conflict of interest. The founding sponsors had no role in the design of the study; in the collection, analyses, or interpretation of data; in the writing of the manuscript; or in the decision to publish the results.

References

1. IATA—Carbon-Natural Growth by 2020. Available online: http://www.iata.org/pressroom/pr/Pages/2009-06-08-03.aspx (accessed on 13 December 2016).
2. Reed, R.C. *The Superalloys: Fundamentals and Applications*; Cambridge University Press: Cambridge, UK, 2006.
3. Miller, R.F.; Ansell, G.S. Low Temperature Mechanical Behavior of Ni–15Cr–Al–Ti–Mo Alloys. *Metall. Trans. A* **1977**, *8*, 1979–1991. [CrossRef]
4. Maniar, G.N.; Bridge, J.E.; James, H.M.; Heydt, G.B. Correlation of Gamma-Gamma Prime Mismatch and Strengthening in Ni/Fe-Ni Base Alloys Containing Aluminum and Titanium as Hardeners. *Metall. Trans. A* **1970**, *1*, 31–42.
5. Xu, Y.; Zhang, L.; Li, J.; Xiao, X.; Cao, X.; Jia, G.; Shen, Z. Relationship between Ti/Al Ratio and Stress-Rupture Properties in Nickel-Based Superalloy. *Mater. Sci. Eng. A* **2012**, *544*, 48–53. [CrossRef]
6. Guo, E.C.; Ma, F.J. The Strengthening Effect of Niobium on Ni–Cr–Ti Type Wrought Superalloy. In Proceedings of the Fourth International Symposium on Superalloys, Champion, PA, USA, 21–25 September 1980; pp. 431–438.
7. Mishima, Y.; Ochiai, S.; Hamao, N.; Yodogawa, M.; Suzuki, T. Solid Solution Hardening of Nickel—Role of Transition Metal and B-subgroup Solutes—. *Trans. Jpn. Inst. Met.* **1986**, *27*, 656–664. [CrossRef]
8. Reed, R.C.; Tao, T.; Warnken, N. Alloys-By-Design: Application to Nickel-Based Single Crystal Superalloys. *Acta Mater.* **2009**, *57*, 5898–5913. [CrossRef]
9. Zhu, Z.; Höglund, L.; Larsson, H.; Reed, R.C. Isolation of Optimal Compositions of Single Crystal Superalloys by Mapping of a Material's Genome. *Acta Mater.* **2015**, *90*, 330–343. [CrossRef]

10. Morinaga, M.; Yukawa, N.; Adachi, H.; Ezaki, H. New PHACOMP and Its Applications to Alloy Design. In Proceedings of the Fifth International Symposium on Superalloys, Champion, PA, USA, 7–11 October 1984; pp. 523–532.
11. Shi, Z.; Liu, S.; Yue, X.; Wang, X.; Li, J. Effect of Nb content on Microstructure Stability and Stress Rupture Properties of Single Crystal Superalloy Containing Re and Ru. *J. Cent. South Univ.* **2016**, *23*, 1293–1300. [CrossRef]
12. Rae, C.M.F.; Reed, R.C. The precipitation of Topologically Close-Packed Phases in Rhenium-Containing Superalloys. *Acta Mater.* **2001**, *49*, 4113–4125. [CrossRef]
13. Singh, A.R.P.; Nag, S.; Chattopadhyay, S.; Ren, Y.; Tiley, J.; Viswanathan, G.B.; Fraser, H.L.; Banerjee, R. Mechanisms Related to Different Generations of γ' Precipitation during Continuous Cooling of a Nickel Base Superalloy. *Acta Mater.* **2013**, *61*, 280–293. [CrossRef]
14. Sarosi, P.M.; Wang, B.; Simmons, J.P.; Wang, Y.; Mills, M.J. Formation of Multimodal Size Distributions of γ' in a Nickel-base Superalloy during Interrupted Continuous Cooling. *Scr. Mater.* **2007**, *57*, 767–770. [CrossRef]
15. Radis, R.; Schaffer, M.; Albu, M.; Kothleitner, G.; Pölt, P.; Kozeschnik, E. Multimodal Size Distributions of γ' Precipitates during Continuous Cooling of UDIMET 720Li. *Acta Mater.* **2009**, *57*, 5739–5747. [CrossRef]
16. Raynor, D.; Silcock, J.M. Strengthening Mechanisms in γ' Precipitating Alloys. *Metal Sci. J.* **1970**, *4*, 121–130. [CrossRef]
17. Reppich, B. Some New Aspects Concerning Particle Hardening Mechanisms in γ' Precipitating Ni-Base Alloys—I. Theoretical Concept. *Acta Metall.* **1982**, *30*, 87–94. [CrossRef]
18. Jackson, M.; Reed, R.C. Heat Treatment of UDIMET 720Li: The Effect of Microstructure on Properties. *Mater. Sci. Eng. A* **1999**, *259*, 85–97. [CrossRef]
19. Collins, D.; Stone, H. A Modelling Approach to Yield Strength Optimisation in a Nickel-Base Superalloy. *Int. J. Plast.* **2014**, *54*, 96–112. [CrossRef]
20. Galindo-Nava, E.I.; Connor, L.D.; Rae, C.M.F. On the Prediction of the Yield Stress of Unimodal and Multimodal γ' Nickel-Base Superalloys. *Acta Mater.* **2015**, *98*, 377–390. [CrossRef]
21. Collins, D.M.; Crudden, D.J.; Alabort, E.; Connolley, T.; Reed, R.C. Time-Resolved Synchrotron Diffractometry of Phase Transformations in High Strength Nickel-Based Superalloys. *Acta Mater.* **2015**, *94*, 244–256. [CrossRef]
22. Mitchell, R.J.; Preuss, M.; Hardy, M.C.; Tin, S. Influence of Composition and Cooling Rate on Constrained and Unconstrained Lattice Parameters in Advanced Polycrystalline Nickel-Base Superalloys. *Mater. Sci. Eng. A* **2006**, *423*, 282–291. [CrossRef]
23. Baldan, A. Review Progress in Ostwald Ripening Theories and Their Applications to the γ'-Precipitates in Nickel-Based Superalloys. *J. Mater. Sci.* **2002**, *37*, 2379–2405. [CrossRef]
24. Ricks, R.A.; Porter, A.J.; Ecob, R.C. The Growth of γ' Precipitates in Nickel-base Superalloys. *Acta Metall.* **1983**, *31*, 43–53. [CrossRef]
25. Qiu, C.L.; Andrews, P. On the Formation of Irregular-Shaped Gamma Prime and Serrated Grain Boundaries in a Nickel-Based Superalloy during Continuous Cooling. *Mater. Charact.* **2013**, *76*, 28–34. [CrossRef]
26. Chen, Y.; Prasath Babu, R.; Slater, T.J.A.; Bai, M.; Mitchell, R.; Ciuca, O.; Preuss, M.; Haigh, S.J. An Investigation of Diffusion-Mediated Cyclic Coarsening and Reversal Coarsening in an Advanced Ni-Based Superalloy. *Acta Mater.* **2016**, *110*, 295–305. [CrossRef]
27. Zhao, X.; Duddu, R.; Bordas, S.P.A.; Qu, J. Effects of Elastic Strain Energy and Interfacial Stress on the Equilibrium Morphology of Misfit Particles in Heterogeneous Solids. *J. Mech. Phys. Solids* **2013**, *61*, 1433–1445. [CrossRef]